Surface chemistry of ion beam modified native titania/Ti interfaces examined using X-ray photoelectron spectroscopy

Pascal Bargiela, Vincent Fernandez, David Morgan, Mireille Richard-Plouet, Neal Fairley, Jonas Baltrusaitis

Results in Surfaces and Interfaces 15 (2024) 100231

Contents lists available at ScienceDirect

Results in Surfaces and Interfaces

journal homepage: www.elsevier.com/locate/rsurfi

Surface chemistry of ion beam modified native titania/Ti interfaces examined using X-ray photoelectron spectroscopy

Pascal Bargiela [a,b], Vincent Fernandez [c], David Morgan [d,g], Mireille Richard-Plouet [c], Neal Fairley [e], Jonas Baltrusaitis [f,*]

[a] The Institute for Research on Catalysis and the Environment of Lyon (IRCELYON), 2 Avenue Albert Einstein, 69626, Villeurbanne, France
[b] Universite de Pau et des Pays de l'Adour, E2S UPPA, CNRS, IPREM, Pau, France
[c] Nantes Université, CNRS, Institut des Matériaux Jean Rouxel, IMN, F-44000, Nantes, France
[d] Translational Research Hub, Cardiff University, Maindy Road, Cardiff, CF24 4HQ, United Kingdom
[e] Casa Software Ltd, Bay House, 5 Grosvenor Terrace, Teignmouth, Devon, TQ14 8NE, United Kingdom
[f] Department of Chemical and Biomolecular Engineering, Lehigh University, 111 Research Drive, Bethlehem, PA, 18015, USA
[g] HarwellXPS – EPSRC National Facility for Photoelectron Spectroscopy, Research Complex at Harwell (RCaH), Didcot, Oxon, OX11 0FA, United Kingdom

ARTICLE INFO

Keywords:
Lineshape
PCA
Oxide
Carbide
Titanium
XPS
Ion beam

ABSTRACT

It is often assumed in X-ray Photoelectron Spectroscopy that binding energy shifts are synonymous with changes in the chemical state of an atom and the chemical state can be described in terms of oxidation state and stoichiometry of the elements in a material that correlates with photoemission peaks. However, when an atom is bonded into a crystal lattice, the shapes and binding energy of photoemission may not match the expected stoichiometry when measured by XPS, even though shifts in binding energy suggest new oxidation states. In this work, a set of experiments is presented, in which Ar^+ and He^+ ions of different energies modify the native oxide on a titanium foil which yields XPS spectra that are not easily open to analysis by conventional peak models. In the course of analyzing these complex photoemission data by linear algebraic methods, the prospect emerged that XPS is suggesting that sputtering a native oxide may be providing insight into structural perturbation in addition to the stoichiometry-type changes to the native oxide.

1. Introduction

Titanium oxides are of significant fundamental and practical interest, especially in environmental and energy applications (Byrne et al., 2018; Pelaez et al., 2012). Their high stability and semiconducting properties have been of perennial interest in the field of environmental (photo) catalysis (Fujishima et al., 2008) and electrocatalysis (Feng et al., 2018). Due to its wide bandgap, however, titanium dioxide (TiO_2) is routinely modified with the dual purpose of improving its light-absorbing properties and generating Ti^{3+} centers where oxygen vacancies enhance electrical conductivity and promoting both electron transfer and hydrogen desorption, yielding active hydrogen evolution catalysts in alkaline media (Feng et al., 2018). Hence, understanding the evolution of titania surfaces during their modification during synthesis, activation or cycling during (electro)catalytic reactions is of paramount importance for the rational engineering of functional materials for energy and the environment. Ion beam modification of titanium dioxide (TiO_2) thin films and particles has emerged as a dry method to obtain surfaces with improved response properties (Sumita et al., 1999; Bala et al., 2020; Tuckute et al., 2019) through the introduction of both chemical and morphological changes in the surface and near-surface region of a sample (Mohanta et al., 2015; Zhan et al., 2021). It is well known, the rutile polymorph of TiO_2 forms at temperatures above 600 °C, however, anatase films formed at lower temperatures (<500 °C) can be transformed into rutile through argon ion (Ar^+) beam irradiation (Sumita et al., 1999), while implantation of low-energy Ar^+ and N^+ ions has been used to cause the formation of defect energy levels in the bandgap or narrow it to shift the absorption into the visible light spectrum (Fernandes et al., 2009). Finally, low-energy ion beams have been shown to induce both chemical and physical transformations, such as the fusion of TiO_2 nanoparticles (Majhi et al., 2022) or N^+-assisted crystallization of TiO_2 nanotubes (Haryński et al., 2023). Other examples include significant structural modification of the top surface layers of Ti- and O-bearing compounds, such as potassium titanyl arsenate, $KTiOAsO_4$,

* Corresponding author.
E-mail address: job314@lehigh.edu (J. Baltrusaitis).

https://doi.org/10.1016/j.rsurfi.2024.100231
Received 3 April 2024; Received in revised form 13 May 2024; Accepted 15 May 2024
Available online 16 May 2024

with 1.5 eV Ar^+ beam by breaking the weaker chemical bond, inducing partial surface amorphization and essential energy redistribution of the valence electronic states (Ramana et al., 2007; Atuchin et al., 2008).

It is well known that the surface chemistry of reduced TiO_2 is complex due to the presence of the multiple integral and fractional valence states following exposure to an ion beam (Mohanta et al., 2015; Zhan et al., 2021; Pabón et al., 2015; Mens and Gijzeman, 1996), all of which manifest as a series of overlapping peaks in all Ti core levels, with the most intense Ti 2p core-level commonly utilized for data analysis. This necessitates complex spectral assignments to unstable or metastable titania species, such as Ti_2O_3 or TiO, which have spectra that cannot be unambiguously assigned using literature references alone.

XPS-measured binding energy shifts indeed manifest themselves as new peaks or shoulders to the peaks. These can be viewed as a result of the local potential of the atom due to its oxidation state but, in reality, their assignment is much more complex since initial- and final-state contributions to the core level shifts exist (Egelhoff, 1987), as well as less explored structural deformation effects (Pasquarello et al., 1996). A large number of previous studies have attempted to elucidate the surface chemistry of TiO_2 using XPS, see for example (Diebold, 2003; Sayers and Armstrong, 1978; FUJISHIMA et al., 2008). Biesinger *et al.* investigated the Ti 2p region of heat-treated Ti-apatite and inferred four doublets assignable to Ti^{4+}, Ti^{3+}, Ti^{2+} and metallic Ti (Biesinger et al., 2010) while noting the assignment of $Ti^{3+}$and Ti^{2+} in the literature is inconsistent. As summarized by Greczynski and Hultman (2016), Ti $2p_{3/2}$ binding energy values for chemical states of titanium decrease from *ca.* 459 to 455 eV as the oxidation state decreases from TiO_2 to Ti_2O_3 to TiO. The authors utilized titanium nitride (TiN) and systematically oxidized it through air exposure at increasing temperatures, obtaining a self-consistent model that accounted for Ti 2p binding energy values, but also did not neglect the O 1s and C 1s signals of the oxide and surface carbonaceous species. Earlier studies investigated Ti oxidation states through the controlled oxidation of titanium foil. Carley *et al.* observed, using angular resolved XPS, that Ti^{2+} and Ti^{3+} were preferentially formed on a metal-oxide interface whereas Ti^{4+} states dominated at the titanium oxide-gas interface (Carley et al., 1987). Intermediate oxidation states and the corresponding oxides, such as Ti_2O_3 to TiO mixed with TiO_2 were found to be thermodynamically stable up to a few Ångstrom oxide thickness (Roberts and Tomellini, 1992). Ion and electron techniques, on the other hand, when commonly applied to modify TiO_2 surfaces, can potentially not only reduce the oxide but also perform chemical reactions. A related example was described by Mens and Gijzeman where electron beam modification of the TiO_2 surface not only resulted in a loss of surface oxygen via an electron-stimulated desorption process but also resulted in graphitic carbon deposition on the surface from residual chamber gases (Mens and Gijzeman, 1996). Consequently, ion modification of the TiO_2 surface can result in a very complex chemical composition with straightforward peak energy assignments not always leading to the correct surface chemistry interpretation.

A completely different approach to XPS data analysis of complex native transition metal oxide surfaces has recently been demonstrated using a guided Principal Component Analysis (PCA) or linear least Squares (LLS) analysis that utilized a multi-spectral region approach. In particular, complex native films on Fe foil have been modified using ion beams to systematically invoke chemical changes (Fairley et al., 2023). Fe 2p, O 1s and C 1s regions were merged into a single spectrum and interpreted as component spectra starting with abstract factors (AFs) derived from PCA (Fernandez et al., 2023). Further, a film of TiO_2 deposited using plasma-enhanced chemical vapor deposition (PECVD) on a silicon substrate was modified with ion beams and the results suggested that spectral features apparent in the resulting XPS spectra, while indicating changes in sample surface properties, did not show any changes in the stoichiometry of the material (Bargiela et al., 2024). In particular, while a reduced titanium peak appeared in the Ti 2p region at *ca.* 457 eV for the surface sputtered with 500 eV argon ions, the resulting surface chemistry did not change significantly. This observation implies that XPS peak assignments, based on the data envelope alone, to reduced crystalline oxides, such as Ti_2O_3 using classical binding energy arguments are not always accurate. In the current work, the experiments were designed to provide XPS spectra from complex native titania films on titanium foil that evolved in shape with sputter times in a form suitable for detailed spectral analysis. By combining spectra measured using argon and helium ions over ion beam energies to include 200 eV (argon), 1 keV (both argon and helium) and 2 keV (both argon and helium), it was possible to construct a set of curves that form the components in a peak model used to fit spectra with the precision expected for data of this nature. This set of component curves includes spectroscopic shapes with chemical interpretation, which can be used to understand the response of a Ti foil sputtered with a range of ion beams to obtain an improved understanding of the surface properties of TiO_2 materials.

2. Experiments and methods

Spectra used in this study were acquired using three different instruments. The first two were supplied by Thermo Scientific™ (K-Alpha$^+$ and Nexsa G2), while the third instrument was a Kratos Axis Nova. The role of each spectrometer is detailed in the proceeding sections. Acquisition parameters for the sputter experiments were copied between the two Thermo Scientific™ instruments. Spectra measured using these two Thermo Scientific™ instruments were sufficiently similar in characteristics to permit the use of the same component spectra, derived from these data sets, for all spectra. However, while spectra measured using the Kratos instrument were similar to the spectra acquired from the Thermo Scientific™ instruments, differences in energy resolution prevented a direct application of the component spectra computed between systems.

2.1. Monoatomic ion beam experiments

Spectra were acquired using a Thermo Scientific™ Nexsa G2 X-Ray photoelectron spectrometer equipped with an EX06 monatomic ion source. The titanium foil (Aldrich, thickness 0.5 mm, 99.9% trace metals, ref 348805), used for analysis was mounted in direct electrical contact with the sample stage and consequently, no charge compensation was used during the measurements. Data was acquired using Thermo Scientific™ Avantage.

Experiments were performed by interleaving acquisitions by XPS and subsequent irradiation with ions. XPS spectra were acquired to include energy intervals aimed at collecting photoemission signals for C 1s, N 1s, O 1s, Ti 2s, Ti 2p, Ti 3s, and an interval covering the Ti 3p and valence band. The exact protocol used to perform these experiments took three forms. The initial experiments involved sputtering the Ti foil, at a new sample position for each experiment, using Ar^+ ions. In these measurements, three replicate experiments were performed using 30-s cycles of ion sputtering using Ar^+ ions with energies of 200 eV, 1 keV and 2 keV, or He^+ ions with energies of 1 keV and 2 keV. A separate experiment using 2 keV Ar^+ ions was performed using 240 s per sputter cycle, which was immediately followed, by an iteration of 30 XPS measurements.

Energy resolution defined as pass energy (PE) of 30 eV and electron lens-column forming an image at the entrance aperture was used to acquire XPS spectra. The total acquisition time for each XPS cycle of measurements was 3.9 min, during which the ion beam was prevented from irradiating. The XPS analysis was performed using microfocused Al radiation (1486.6 eV), using the 400 μm spot mode, which is an ellipse of *ca.* 600 μm by 400 μm. A raster performed by the ion beam was designed to cover an area multiple times the size of the XPS analysis area. Each sputter experiment involved 40 sputter cycles.

2.2. Argon cluster ion beam measurements

Spectra were acquired using a ThermoFisher Scientific™ K-Alpha$^+$ photoelectron spectrometer equipped with a combined monatomic and gas cluster ion source (MAGCIS). As for the monatomic sputtering experiments, titanium foil (Goodfellow UK, thickness 0.025 mm, 99.6%+ purity) was mounted using copper clips attached to each corner of the foil to ensure direct electrical contact with the sample holder and stage. No charge compensation was used during the acquisition of spectra.

Identical acquisition parameters for the data collected on the Nexsa G2 system (spot size, PE, region width, etc) were used through sharing of the *Avantage* acquisition parameter file. However, the ion gun was operated in its cluster mode, using an accelerating voltage of 8 keV and cluster sizes obeying a Gaussian distribution with the most likely size of 500 (Ar_{500}) and 150 (Ar_{150}). The expected energy per argon atom for these clusters is 16 and 53.3 eV respectively. The base pressure of the system was 2×10^{-9} mbar, rising to *ca.* 5×10^{-7} mbar during sputtering experiments.

2.3. Sample surface reoxidation measurement

Data were acquired using a Kratos Axis Nova. The base pressure of the instrument was 2.6×10^{-10} mbar. The energy resolution for the instrument is defined by a fixed analyzer transmission mode. Data collection was performed using PE 40 eV and transfer lens modes with an analysis area at the sample ca. 800 μm × 800 μm slot mode, field of view 1 (FoV1). Before acquiring spectra, the surface of the titanium foil sample was cleaned using a monoatomic argon ion gun at 4 keV. The overall instrument resolution at PE 40 eV measured using the Fermi edge was 0.55 ± 0.02eV. The argon gas differential pressure was 5×10^{-6} mbar. During sputtering with a monoatomic argon beam, the pressure in the analysis chamber was *ca.* 7×10^{-8} mbar and reached a surface oxygen content of *ca.* 3%. After cleaning the Ti sample, the residual gas pressure in the analysis chamber was 6.8×10^{-9} mbar. High-resolution O1s, C1s, Ti2p and Ar 2p spectra were recorded in each cycle. Each cycle took 8 min 44 s, with a total of 122 cycles recorded.

2.4. Data analysis

Data were analyzed using CasaXPS version 2.3.26 (Fairley et al., 2021). For the Thermo Scientific data, integrated peak areas were corrected for the instrument transmission function and relative sensitivity of the photoemission signal using Scofield cross-sections (Scofield, 1976). No escape depth correction to the raw signal was performed since the native oxide layer of titanium foil is sufficiently thick (5–6 nm) (Jenko et al., 2018) to be considered a bulk material.

2.5. Data analysis concepts using linear algebra, Principal Component Analysis and abstract factors

Techniques based on linear algebra were used to reduce raw spectra to component curves capable of reproducing all Ti 2p and O 1s spectra in all data sets with precision consistent with noise in pulse-counted data. For a full description of the method, the reader is referred to recent work by Garland et al. (2022). Briefly, a set of linearly independent vectors - spectral components - were derived from Ar^+ and He^+ modified samples through the determination of the maximum number of significant components using PCA. The derivation of the suitable set of vectors is based on prior knowledge of titanium oxide species (Biesinger et al., 2010; Greczynski and Hultman, 2016; Kurtz and Henrich, 1998). LLS fitting was then used to obtain a final solution by minimizing the figure of merit. Owing to the relative simplicity of signal from C 1s spectra, results presented that include a chemical state involving carbon were obtained through the use of nonlinear optimization with Voigt lineshapes. While PCA was essential for the analysis of data, it should be emphasized that PCA is not directly used in the partitioning of signal into the chemical state, but rather is a tool that permits mathematical intuition to be applied, in conjunction with knowledge about XPS and the sample and its chemistry, to construct the component spectra.

3. Results and discussion

High-resolution O 1s, Ti 2p and C 1s spectra of native oxide films on titanium foil, irradiated with a 1 keV He^+ beam are shown in Fig. 1 a-c. The O 1s signal was centered at 530.5 eV and ascribed to Ti–O bonds in TiO_2 (Diebold and Madey, 1996), additional peaks to the higher binding energy side of the lattice oxide due to surface hydroxylation and C–O/C═O/C–O–C contamination, the latter consistent with the peaks above *ca.* 285 eV in the C 1s spectra. A small C 1s signal at 281.9 eV is also noted and ascribed to titanium carbide. Analysis of the Ti 2p spectra identified TiO_2 as the major species, with an associated Ti $2p_{3/2}$ peak at 459.3 eV (Diebold and Madey, 1996), while a small contribution from metallic Ti at 453.5 eV is also observed. The extended valence band region (not shown) exhibits peaks due to Ti 3p at 38 eV, which shifts downward by 3 eV during sputtering, and O 2s and O 2p signals (26 - 23 eV and 10-5 eV respectively) which remained relatively stable (Oku et al., 1999). The peak areas were integrated to extract the relative distribution of the elements as a function of the sputtering time. The intensity of the O 1s peak increased as a function of sputtering time as shown in Fig. 1d, consistent with the removal of the attenuating carbon-containing overlayer. The increase and stabilization in the oxygen signal suggest that the 1 keV He^+ beam did not remove but rather predominantly reduced the oxidation state of the titanium species. Experiments with a 2 keV He^+ beam (not shown) did not result in significant alteration of the spectral patterns.

Results from a similar experiment using a monoatomic 200 eV Ar^+ ion beam are shown in Fig. 2(a and b). When the as-received surface is exposed to argon ions, a well-resolved C 1s peak appears at 281.9 eV and is notably more pronounced than in the equivalent He^+ ion experiments (Fig. 1c). The presence of such a low binding energy C 1s peak is consistent with carbide (Jiang and Rhine, 1991; Luthin and Linsmeier, 2001). While we note the Ti foil has some carbide present initially, we do not discount the possibility of argon ion-induced carbide formation.

To understand the ion-induced changes caused by both Ar^+ and He^+ ions, PCA was applied to the data sets shown in Figs. 1 and 2. Six significant component spectra were identified on Ti 2p and O 1s spectra (Fig. 3a and b) and labeled as ***Ti^{4+}***, ***metal*** and ***Phases 1–4***, where the term phase refers to a significant Ti 2p or O 1s chemical phase AFs obtained from the PCA analysis. Three different component spectra of ***C 1s adventitious***, ***C 1 sputtered*** and ***C 1s carbide*** are shown in Fig. 3c. The latter contained discernible peaks of ***C* 1s C-*Oa*** and ***C* 1s C-*Ob***. By applying these AFs to the 1 keV He^+ sputter experiment (see Fig. 1b), the sputter profile shown in Fig. 3d was generated. Fig. 3e, on the other hand, shows the LLS fit of the six components from Fig. 3a to the Ti foil spectrum following 30 s of sputtering with 1 keV He^+ ions. It can be seen that this particular spectrum is chiefly comprised of ***Ti^{4+}*** and ***Phase 1*** components.

The concept of "physical sense" is put into practice when selecting these components by considering depth profiles such as that in Fig. 3d. In particular, the component curve ***Ti^{4+}*** is justified based on prior knowledge of the Ti^{4+} state (Biesinger et al., 2010) and, in the case of the component spectra ***Metal***, the heuristic that the spectrum for metal should be defined by the point at which the corresponding oxygen photoemission is close to zero. Importantly, both of these component spectra, ***Ti^{4+}*** and ***Metal*** in Fig. 3a, were computed rather than using raw spectra present from any profile. Components ***Phase 1*** through ***Phase 4*** were similarly computed by iterating steps that involved selecting spectral forms. ***Phase 2*** and ***Phase 3*** contained a significant contribution of Ti $2p_{3/2}$ peak at 456.0–458.0 eV while **Phase 1** contained low binding energy shoulder at 458 eV. **Phase 4**, on the other hand, exhibited features of metallic titanium shifted to a higher binding energy side by *ca.* 1 eV. The component spectra labeled ***Phase 4*** can be correlated with

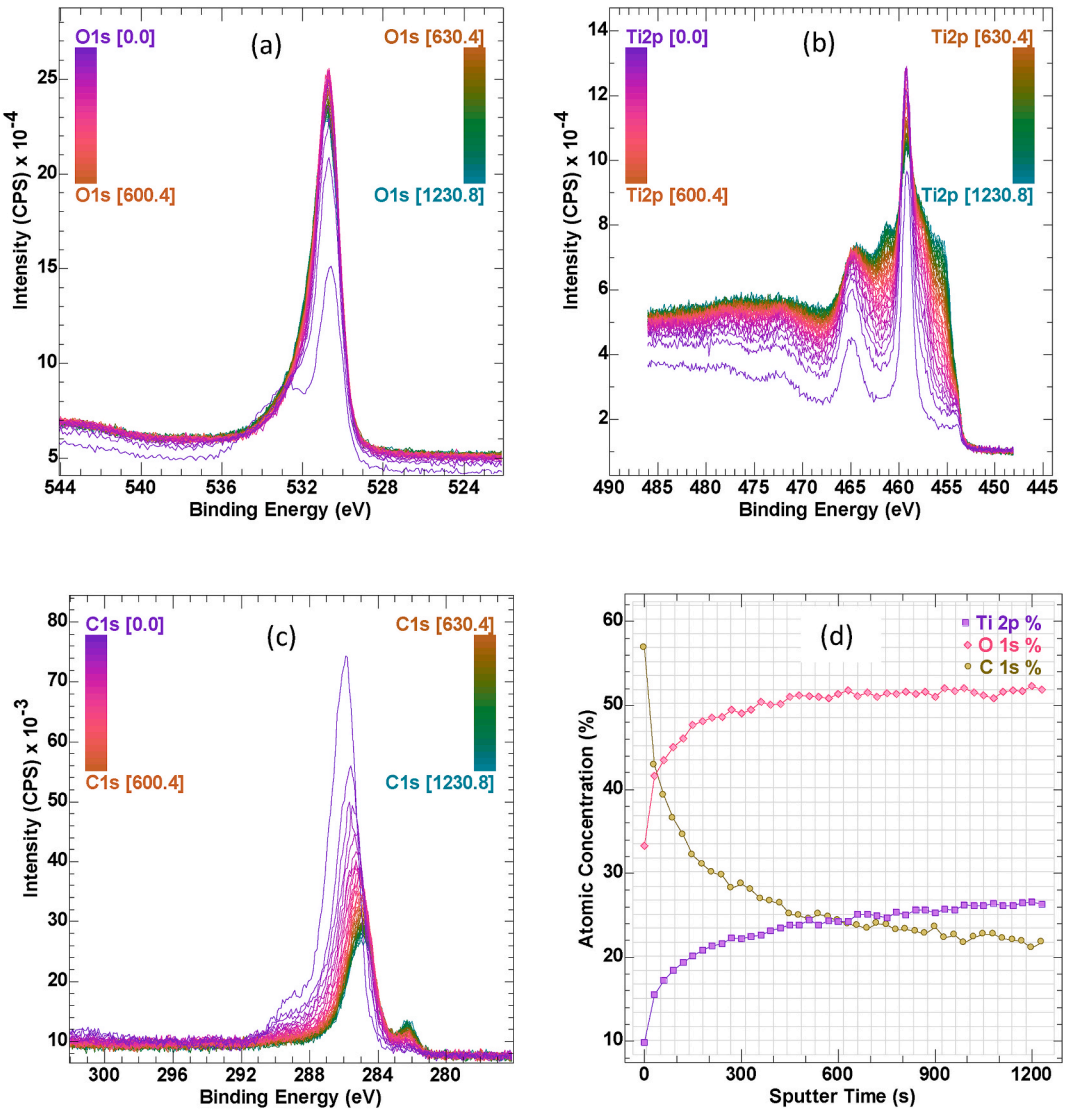

Fig. 1. High resolution (a) O 1s, (b) Ti 2p and (c) C 1s spectra of native titanium oxide film sputtered with 1 keV He^+. (d) Relative atomic concentration profile of carbon, oxygen and titanium. Scale bars represent the time of the acquisition in seconds.

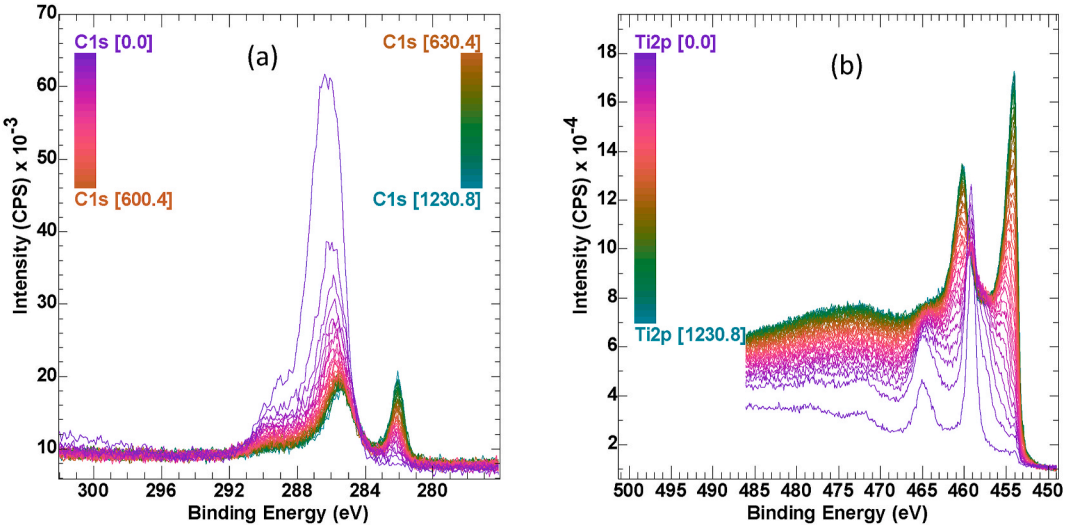

Fig. 2. (a) C 1s and (b) Ti 2p spectra measured between sputter cycles from titanium foil using 200 eV Ar^+ beam.

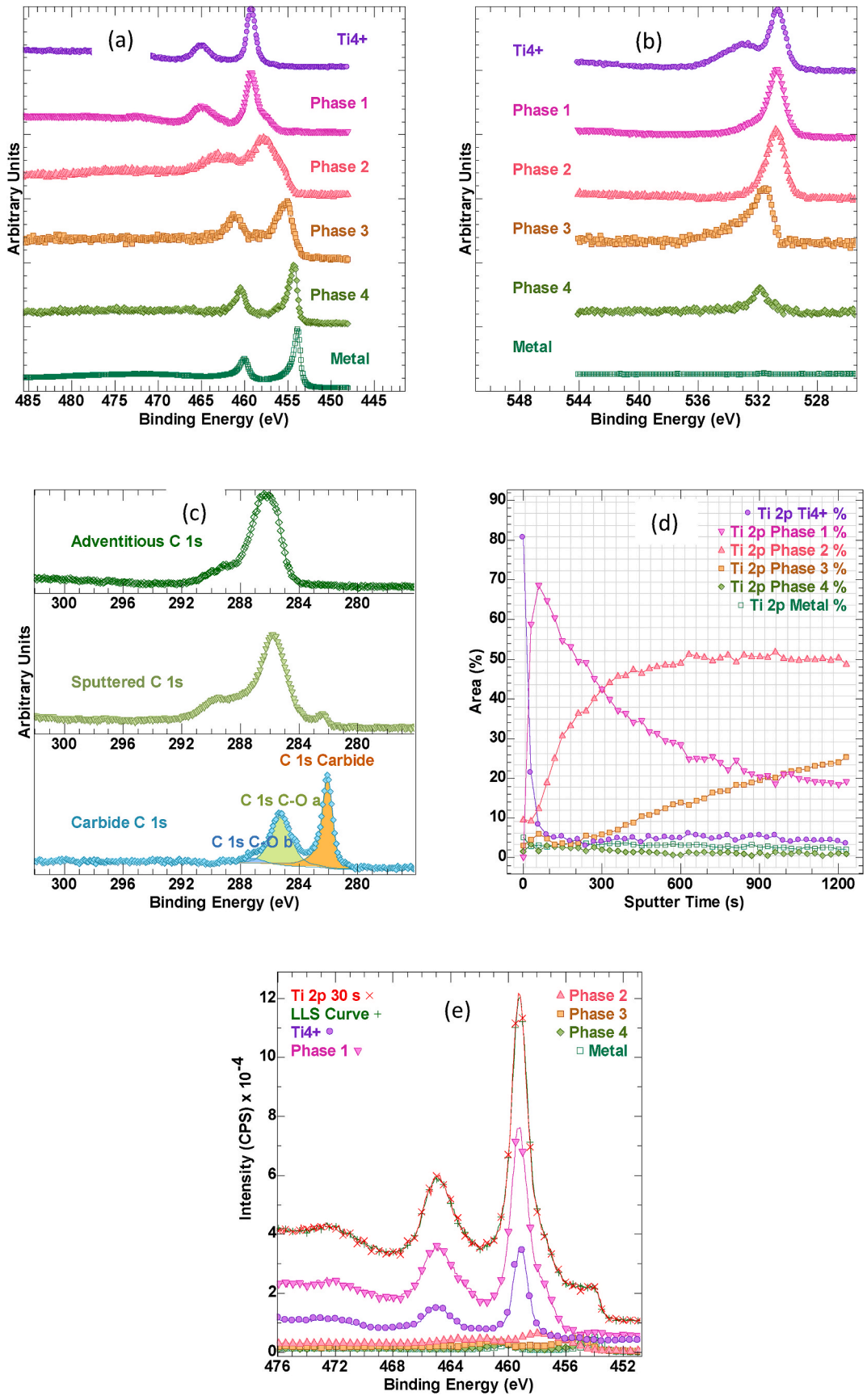

Fig. 3. (a) Ti 2p, (b) O 1s and (c) C 1s component spectra computed from XPS spectra acquired using helium and argon ion beams to modify the Ti foil. (d) The plot of Ti 2p intensity measured during a sputter profile was performed using 1 keV He^+ ions by fitting component spectra in (a) to Ti 2p spectra acquired following 40 sputter cycles of 30 s per cycle. (e) The fit of component curves shown in (a) to Ti 2p spectrum measured from Ti foil following 30 s of sputtering with 1 keV He^+ ions.

titanium carbide, and explain a metallic-like spectrum with an energy difference to that of pure metallic Ti. As already stated, the exact assignment of Ti^{3+} and Ti^{2+} states is difficult (Biesinger et al., 2010), nevertheless, Ti $2p_{3/2}$ peaks at 456.6 and 454.4 eV have previously been assigned to those oxidation states (Gonbeau et al., 1991). Of course, in any ion sputtering study on an oxide surface, preferential sputtering cannot be ignored and will always be present, hence substoichiometric compounds, such as $TiO_{1.5}$ (González-Elipe et al., 1989) will form, or potentially small metallic Ti clusters which could also contribute to **Phase 4** due to particle size effects. Finally, the sputter profiles in Figs. 1 and 2 clearly show that the as-received surface includes a significant adventitious carbon layer. It is therefore expected that due to photoemission escape depth considerations, oxygen and carbon from the contamination layer will contribute to the attenuation of buried material, such as TiO_2, but over-estimate O 1s intensity from the contamination at the surface. Since the contributions to the profiles in Fig. 3c are mostly associated with the initial XPS measurements, component spectra labeled ***Ti*$^{4+}$** and ***Phase 1*** are strongly associated with the top layers of the sample. By contrast, ***Phase 2*** appears after these contamination layers are removed.

For a more informed view of the data, the analyst cannot take the Ti 2p spectra in isolation. Hence the concept of correlating PCA-derived abstract component spectra with information from other photoemission peaks is introduced and utilized by (a) performing O 1s/Ti 2p quantification and (b) observing changes to C 1s spectra during sputter experiments. O 1s/Ti 2p quantification of the phases shown in Fig. 3a and b is presented in Table 1.

The results in Table 1 for ***Ti*$^{4+}$** and ***Phase 1*** are therefore thought to be a consequence of oxygen from the contamination layer interfering with the titanium-to-oxygen ratio resulting in O 1s/Ti2p in the ***Ti*$^{4+}$** phase of 4.0. Consequentially, both ratios for ***Ti*$^{4+}$** and ***Phase 1*** are not representative of the native oxide. ***Phase 2***, on the other hand, which might be considered as an ion beam-cleaned surface, is more representative of the sputtered oxide without surface contamination. The ratio of titanium to oxygen in the case of ***Phase 2*** is close to that expected for the stoichiometry of TiO_2. There is the possibility that ***Phase 2*** represents chemical bonds for titanium in a 4+ state but perturbed by defects to the crystal structure induced by sputtering with an ion beam. Interestingly, a similar lineshape reported by Kurtz and Henrich was assigned to Ti_2O_3 (Kurtz and Henrich, 1998; Baer and Shard, 2020; Chang et al., 2018), which however could be a mixture of TiO_2 and Ti_2O_3. To date, however, the most detailed work that described freshly cleaved crystalline Ti_2O_3 was by Chambers and coworkers (Chambers et al., 2017) the spectral shape agrees more with ***Phase 2*** observed in Fig. 3a of this work. In the present work, however, ***Phase 3*** represents, both the peak position and O 1s/Ti 2p ratio of 1.4 titanium in the binding state and chemical configuration of Ti_2O_3 (but not necessarily that obtained from a single Ti_2O_3 crystal) (Kurtz and Henrich, 1998; Baer and Shard, 2020; Chang et al., 2018). **Phase 4** exhibits an O 1s/Ti 2p ratio of 0.6, lower than the purported TiO. An alternative explanation is that ***Phases 2*** and ***3*** represent dynamically derived combinations of Ti^{4+} rich and Ti metal phases.

Table 1
The ratio of corrected peak areas for O 1s intensity to Ti 2p intensity for component spectra Fig. 3a and b. In parenthesis, O 1s/Ti 2p values are provided for the quantification performed using Voigt lineshapes (for ***Ti*$^{4+}$** and ***Phase 1***) and using regions (***Phase 2***) after C–O contributions were factored out in the O 1s region.

Component Spectra	Ratio O 1s/Ti 2p
Ti^{4+}	4.0 (2.0)
Phase 1	2.8 (2.0)
Phase 2	2.1 (2.1)
Phase 3	1.4
Phase 4	0.6
Metal	0.0

The appearance of the 281.9 eV peak in Figs. 1 and 2 is inferred in the latter stages of ion beam sputtering suggesting that ***Phase 4*** can also be related to the Ti–C bonds. The etched clean titanium was measured by XPS without further sputter cycles. The result of monitoring C 1s over 30 acquisition cycles in Fig. 4a was that the carbide signal grew with time, suggesting sputtering provided the seed for the formation of bonded carbon and titanium. It is also instructive to note this relationship between titanium and carbon when the as-received surface is sputtered using helium ions, is not so apparent as is observed when sputtering with argon ions. Fig. 3d shows that He^+ sputtering does not add to the intensity for either ***Phase 4*** or ***Metal*** component spectra. Further, helium ions fail to remove carbon (and oxygen) as shown in Fig. 1d.

The trend in the carbide-type C 1s generally follows the change in ***Phase 4*** intensity as shown in Fig. 4b. Further, ***Ti*$^{4+}$**, ***Phase 1*** and ***Phase 2*** intensities are attenuated with sputter time, while ***Phase 3*** builds with sputter time before attenuating. It is therefore clear, from the profiles presented in Fig. 4a and b, that argon ions with similar energy to helium ions have a profound influence on the sample. Firstly, the momentum for argon ions is far greater than for helium ions with the same energy. Therefore, the stress to the crystal lattice is greater when irradiated with argon ions compared to helium ions. A second difference, is argon ions carry more electrons with more asymmetry in their electron distribution compared to the simple hydrogenic electron configuration of helium ions. The physical size of these electron distributions and defects in the crystal lattice caused by either of these two ions could contribute to changes in the physical properties of the crystal without necessarily altering the stoichiometry for titanium and oxygen ligands. Argon, in particular, when used to sputter a sample embeds into the sample in sufficient concentration to produce photoemission peaks. It is, therefore, reasonable to assume changes to Ti foil due to sputtering with ions, crosses a threshold that is independent of energy, above which titanium enters at least one phase in which delocalized metallic bonds are responsible for the binding energy observed by XPS. It is also plausible that in the absence of sputtering, titanium forms oxides and carbides during the rest period during which XPS is performed. Moreover, Fig. 4 shows that once formed, the carbide-like signal is persistent when sputtering with argon using 30 s sputter cycles regardless of ion beam energy.

3.1. *Re-oxidation in vacuum of titanium foil*

The quality of the vacuum in the analysis chamber can be compared over time by performing an experiment in which a standard titanium foil is sputtered with an ion beam to remove all contaminants and native oxide from the foil, and then allowed to re-oxidize while periodically recording XPS spectra to monitor changes in the sample surface. Measurements of this nature allow the state of the analysis chamber to be compared over time and therefore highlight changes in cleanliness that might influence the outcomes for analyses of samples for which characterization by XPS is desired, especially for highly reactive materials (Morgan, 2023).

The high-resolution O 1s, Ti 2p, C 1s and Ar 2p spectra during the process of reoxidation after initial sputtering with a 4 keV Ar^+ beam are shown in Fig. 5. It can be seen that the intensity of the O 1s peak grows concomitantly with the 285.0–288.0 eV region of C 1s. The Ti 2p region only experiences minor changes to the fully reduced titanium peak at 454.0 eV suggesting no oxidation.

PCA analysis was performed on the spectra shown in Fig. 5 and only three AFs were present. These AFs are shown in Fig. 6a and were used to construct the sputter time profile shown in Fig. 6b. These three component curves in Fig. 6a when fitted to spectra from the re-oxidation sequence in Fig. 5b suggest the sputter-cleaned metal surface initially forms an oxide with the average stoichiometry of 3:2 (O 1s/Ti 2p = 1.48) as shown in Table 2, but once the amount of oxygen approaches a steady state, the formation of metal oxide yields a complex structure for the Ti

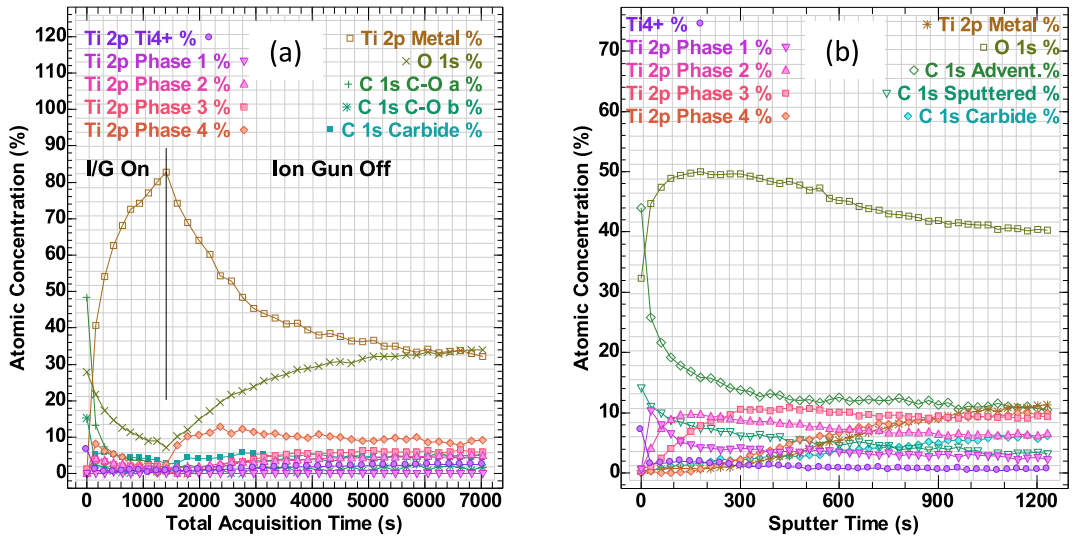

Fig. 4. (a) Ti foil sputtered for 240 s per sputter-cycle, using 2 keV Ar^+ ions for the first 10 XPS measurement cycles, followed by 29 XPS measurement cycles without the use of the ion gun. (b) Ti foil sputtered using 1 keV Ar^+ ions. All profiles are computed by making use of the six component spectra shown in Fig. 3a. Experiments in which argon ions are used to sputter the sample at different locations on the sample.

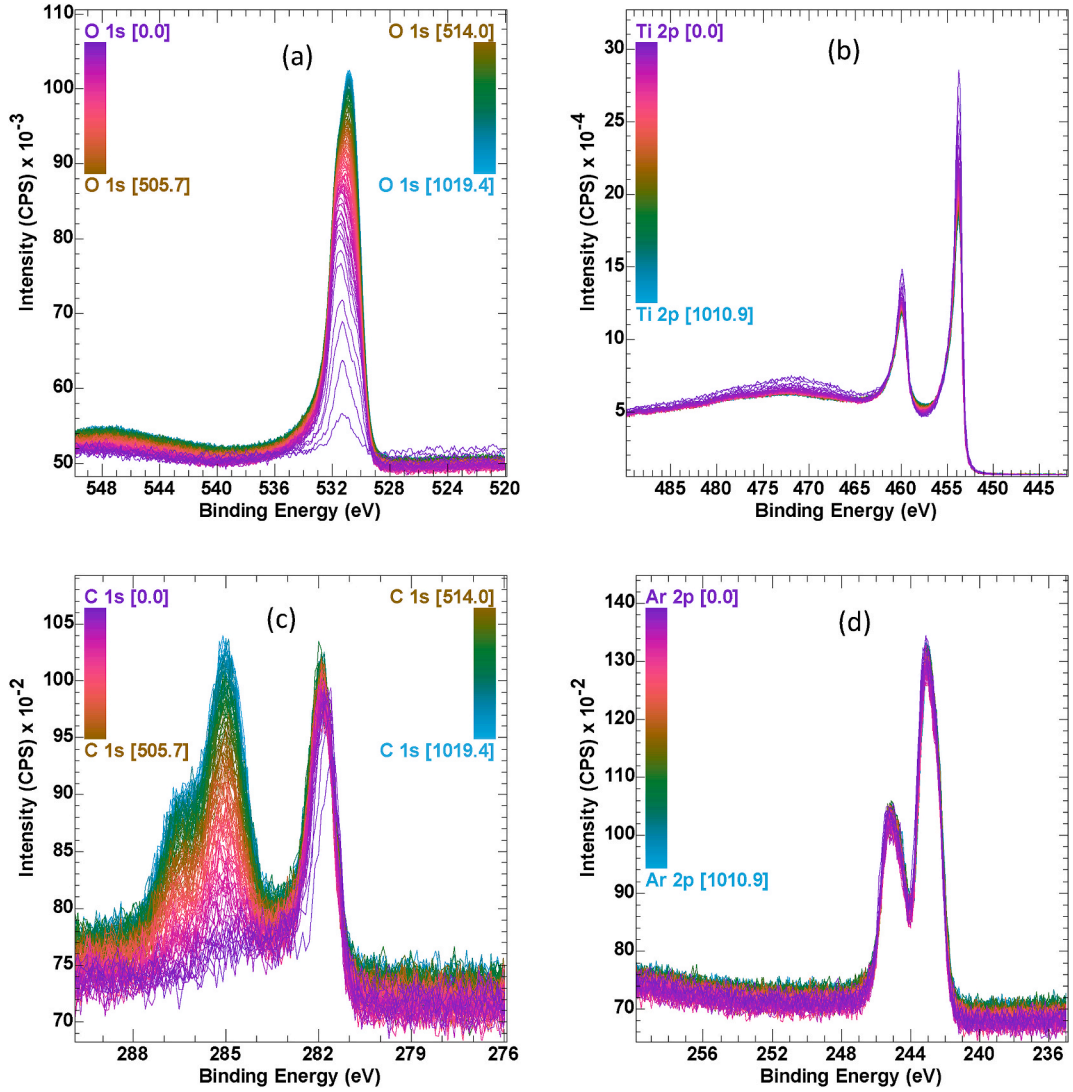

Fig. 5. High resolution (a) O 1s, (b) Ti 2p, (c) C 1s and (d) Ar 2p spectra of native titanium oxide films on titanium foil sputtered with Ar^+ beam at 4 keV reoxidized under natural conditions of chamber contaminant partial pressure.

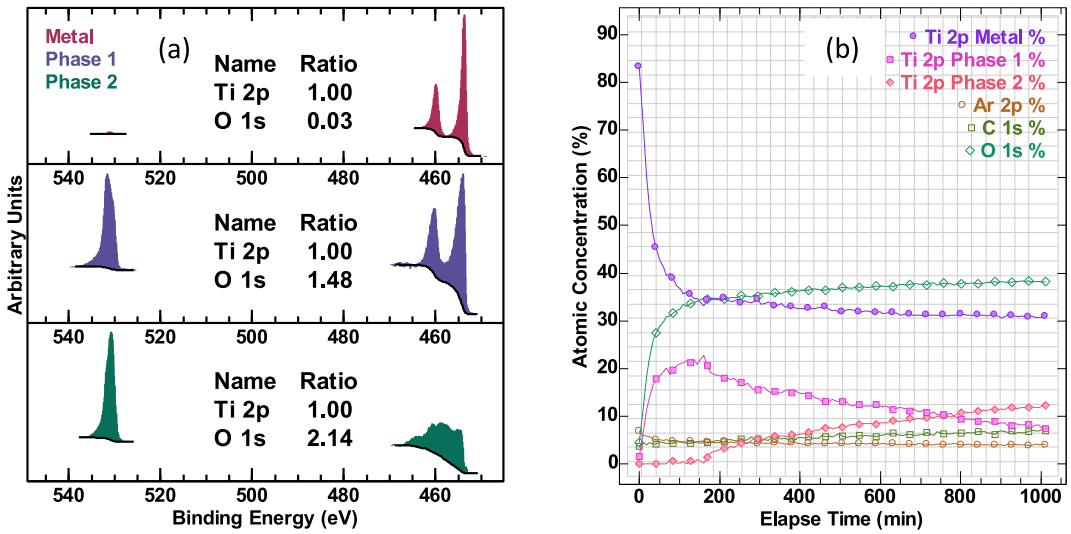

Fig. 6. (a) Component spectra calculated using spectra measured from Ti foil following argon sputtering. The surface analyzed by XPS was sputtered with argon ions until it was no longer possible to remove either carbon or oxygen from the sample. (b) Profile of percentage atomic concentration computed from integration regions defined on Ti 2p, using fits of component spectra in (a) to spectra measured for 1011 min, together with integration regions defined for O 1s, C 1s and Ar 2p.

Table 2
O 1s/Ti 2p ratio calculated from the photoemission curves shown in Fig. 6a.

Component spectra	O 1s/Ti 2p
Metal	0.03
Phase 1	1.48
Phase 2	2.14

2p photoemission with an average stoichiometry close to 2:1. Since the thermodynamically most advantageous phase for titanium oxide is expected to be TiO_2, the shape for photoemission from ***Phase 2*** (Fig. 6a) is further evidence that substoichiometric oxides formed on titanium may yield photoemission peaks with shifts in binding energy and shape atypical of crystalline Ti^{4+}.

The ratios in Table 2 are calculated assuming the material quantified is formed at the interface between the sample surface and the vacuum and that the thickness of the oxide layer is negligible compared to the bulk material. Under these assumptions, attenuation of the O 1s signal relative to Ti 2p, both of which are close in binding energy, is not significant. Further, the instrumental mode used to acquire these data is tuned to permit the measurement of XPS images with identical areas and spatially registered. Therefore, the relative sensitivity of these photoemission peaks is governed by thin film quantification that is best performed using Scofield cross-sections without any escape depth correction. Under this regime for quantification, the estimate for oxygen is thought to be an underestimate, rather than over-estimated, which would be the case if bulk RSFs or Scofield plus escape-depth corrections were included in the calculation of atomic concentration. The estimate for the metal atomic concentration, by the same logic, is underestimated as the metal signal will be attenuated by the growth of an oxide layer (Fig. 6b).

3.2. *Titanium foil response to argon cluster ion beams*

An alternative to monoatomic argon- or helium-ion beams is an ion beam formed from clusters of argon atoms. Clusters with well-defined numbers of atoms-per-cluster, acquire a positive charge and are accelerated towards the sample with identical energy. Argon clusters of different sizes, accelerated by the same voltage, offer a means to deliver to the sample an impulsive force with differing characteristics. In particular, the loosely bound cluster of argon atoms provides an alternative regime, on impact, to monoatomic argon shown in Fig. 2 where forces acting on the surface atoms have greater focus than argon cluster atoms thus affecting the inorganic materials less (Barlow et al., 2014). The spectra presented in Fig. 7 created using argon clusters of differing sizes have more in common with profiles generated by helium ion beams than monoatomic argon ion beams.

These argon-cluster ion guns allow tuning of the ion beam for different applications. Thus, to further investigate the response of native oxides on titanium metal to ion beams, two measurements were performed in which argon clusters of size 150 atoms (Ar_{150}) and 500 (Ar_{500}) atoms were accelerated by 8 keV, yielding 53.3 eV and 16 eV per nucleon in the cluster. The component spectra displayed in Fig. 3a were used to analyze spectra measured during these two experiments involving argon-cluster ion beams. The results of the analysis for XPS spectra measured from surfaces exposed by argon-cluster sputtering, in the form of profiles, are shown in Fig. 8.

In Fig. 8, both profiles were computed to include O 1s atomic concentration, however, to permit greater clarity in the trends observed for C 1s and Ti 2p, the traces presented in Fig. 8 exclude the O 1s response to sputtering. Carbon is more germane to the response of Ti foil to sputtering. Oxygen and other termination chemistry are also likely to contribute to the character of the Ti 2p signal labeled ***Phase 4*** in Fig. 3a. Nevertheless, both traces (***Phase 4*** and ***Carbide***) in Fig. 8 show similar behavior between ***Phase 4*** and the ***Carbide***, particularly as the profile enters a steady state composition following extended sputtering. It should be noted that it is assumed carbon originates from adventitious contamination, therefore during the initial part of these profiles the carbon is at the surface and the growth of carbon defects in titanium initially yields low signal intensity. Hence, the precision with which component spectra for Ti 2p and O 1s are fitted to spectra is compromised by low-intensity signal affecting ***Phase 4*** signal determination. Finally, sputter experiments making use of two different cluster sizes (Ar_{500} and Ar_{150} argon atoms, Fig. 8a and b, respectively) result in different chemistry in the surface layer exposed by the ion beam. The initial surface chemistry is rapidly replaced by similar chemistry in the form of ***Phase 1*** and ***Phase 2***. With each sputter cycle, ***Phase 3*** emerges, which is consistent with both helium- and argon-monoatomic ion beams. One notable difference between these two experiments involving argon-cluster ion beams is that when sputtered with 8 keV Ar_{500} clusters, ***Phase 2*** appears to enter a steady state concentration within the surface, whereas the ***Phase 2*** intensity for 8 keV Ar_{150} clusters attenuates following an initial increase (Fig. 8b). Moreover, sputtering the Ti foil

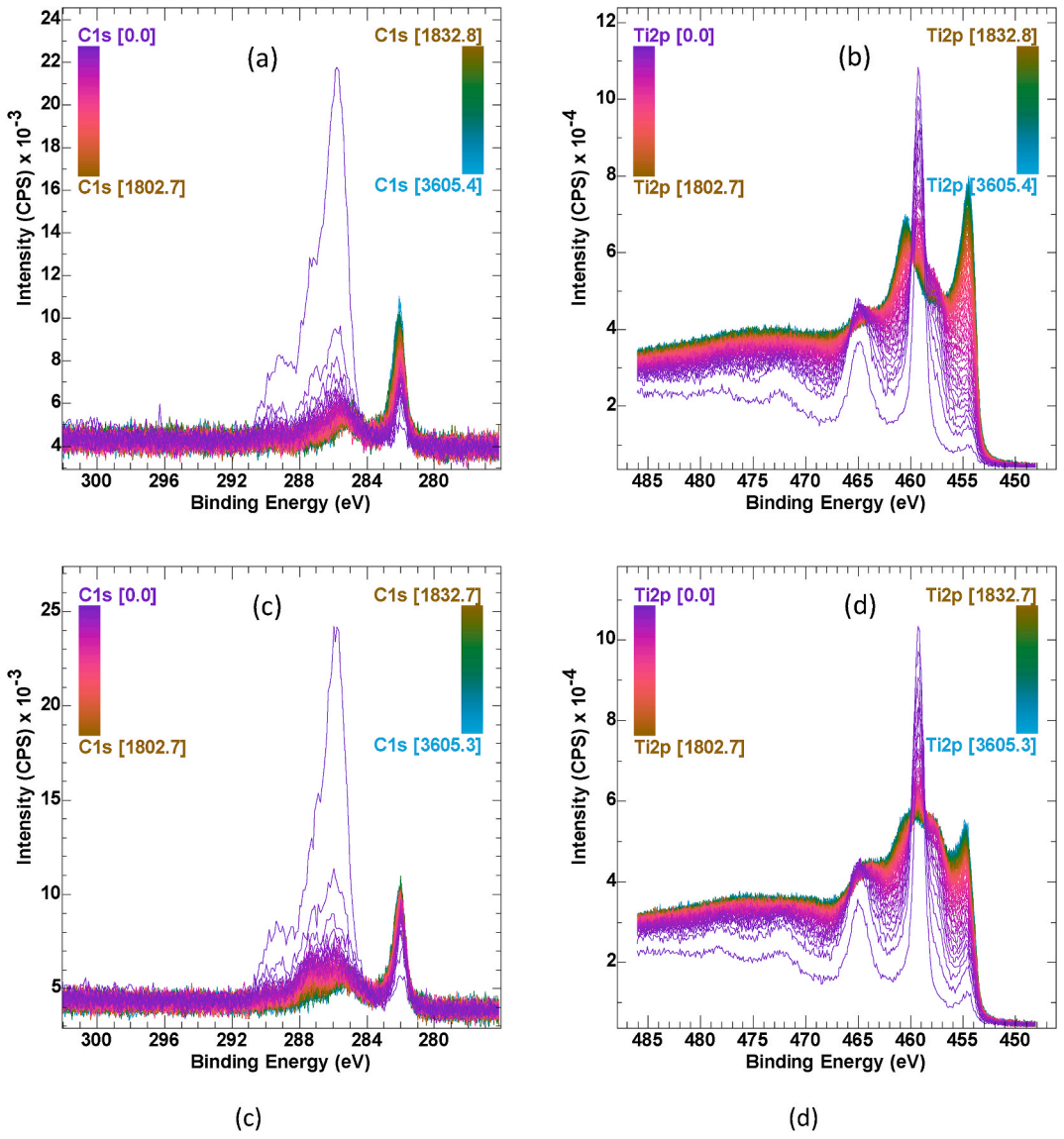

Fig. 7. C 1s and Ti 2p spectra measured between sputter cycles from titanium foil using Ar $^{+}$ cluster beam: (a) and (b) 8 keV Ar_{150}, (c) and (d) 8 keV Ar_{500}.

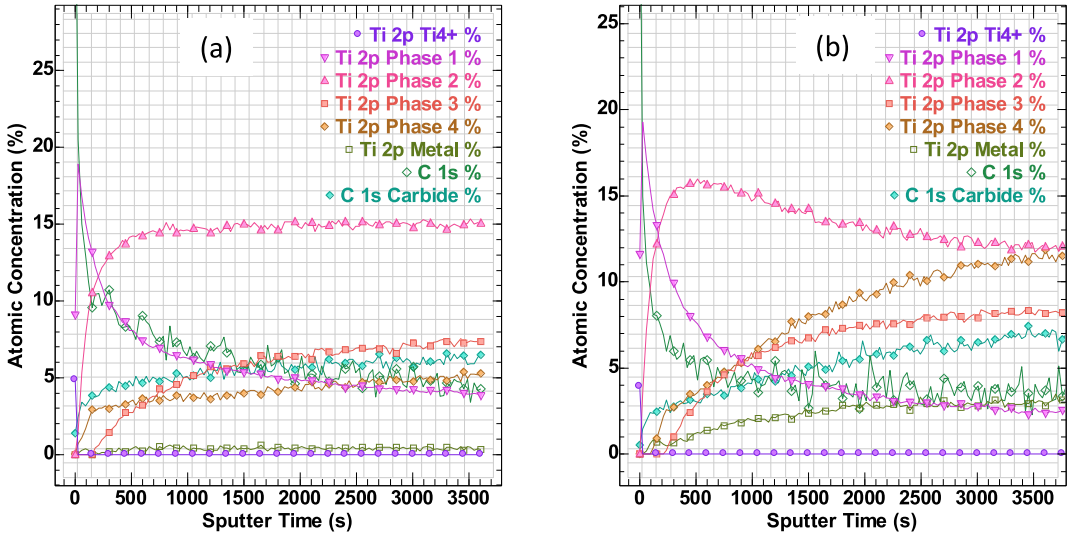

Fig. 8. a) Ti foil sputter experiment using 8 keV, Ar_{500}. B) Ti foil sputter experiment using 8 keV, Ar_{150}. Both profiles are calculated by fitting the component curves in Fig. 3a–O 1s, C 1s and Ti 2p simultaneously.

with 8 keV Ar_{150} clusters compared to 8 keV Ar_{500} clusters, yield in the case of 150 atoms, changes in all phases (as defined by the component spectra in Fig. 3a) that are more pronounced than when sputtering is performed with 500 atom clusters. In particular, sputtering with 8 keV Ar_{500} clusters fails to create a signal (identified by the fitting of the curves in Fig. 3a–O 1s and Ti 2p spectra) that is metal, instead favoring the signal assigned to ***Phase 4***.

When presented with a result that clearly shows a significant difference such as the absence of the phase labeled ***Metal*** in Fig. 8a compared to Fig. 8b, and since these results are obtained by applying component spectra from Fig. 3a to these data in Fig. 8, there is the possibility that the lack of metal signal is an artifact of the linear algebraic solution rather than chemistry. However, in this example, other evidence tends to support the assertion that a metal phase is not created during the sputtering with argon cluster ions constructed from 500 atoms. A strong indicator is a comparison of PCA applied to Ti 2p spectra from these two argon cluster experiments. PCA shows there is, in the case of Ti 2p spectra measured using argon cluster ions with 150 atoms, an additional AF compared to data measured when sputtering with 500 atoms argon-clusters. It is also the case that ***Carbide*** components form regardless of size for argon clusters. It seems reasonable to conclude the results shown in Fig. 8 are correct in that Fig. 8a suggests 8 keV Ar_{500} clusters do not create the metal phase of titanium from native oxide. Thus, these experiments show that it is possible to alter the reduction of oxide by making use of ions ranging from helium, which failed to produce ***Phase 4*** or ***Metal***, to monoatomic argon which creates metal with ease. Cluster source ion beams, depending on cluster size, are capable (500 atoms) of targeting ***Phase 4*** as the lowest oxidation state for titanium, as well as being capable (150 atoms) of attaining ***Phase 4*** and the metal phase of titanium.

4. Conclusions

Experiments performed on Ti foil, using ion beams with different ions and different energies for these ions, allow XPS to provide insight into the environments for titanium that cause changes in lineshapes and shifts in binding energy for photoemission from core-level electrons in titanium. While studying Ti 2p spectra, the origin of material properties and the way changes in material properties influence spectroscopic shapes and binding energies have been considered. There is evidence to suggest structural perturbation induced by sputtering contributes to changes in photoemission peaks that would typically be interpreted as changes to stoichiometry but are perhaps more representative of stresses applied through bonds for titanium that remain coordinated to ligands per the original material. Only when sputtering results in the breaking and reforming of bonds, is it apparent that changes in chemistry correlate with shifts in binding energy for photoemission peaks. In this sense, studying the shapes of photoemission peaks provides insight into the crystal structure as well as chemical state changes.

Of particular interest is the ***Phase 2*** lineshape, similar to which has previously been assigned to the Ti_2O_3 *crystalline* phase (Kurtz and Henrich, 1998; Baer and Shard, 2020; Chang et al., 2018). We now address the question of whether a complex lineshape, that appears with binding energy different from that expected for Ti^{4+}, represents a chemically altered species due to changes in coordination of the metal atom with ligands or are these changes to spectral shapes and nominal binding energies a consequence of deformations in the material, that alter lineshapes and binding energies without altering the oxidation state for the metal. ***Phase 2*** with a shape similar to the lineshape reported by Kurtz and Henrich (1998) and separately by Chambers (Chambers et al., 2017) appears in both sputter experiments and re-oxidation. In both cases, ***Phase 2*** results in an oxygen-to-titanium ratio of 2:1 accompanied by a symmetrical O 1s peak implying no other oxygen-bonded species are present. Reduction experiment ***Phase 3*** and reoxidation experiment ***Phase 1*** both have a nominal oxygen-to-titanium ratio of 3:2 which differ significantly in shape from the lineshape reported by Kurtz and Henrich. Since the lineshapes derived can be linear combinations of the corresponding crystalline phases, it is also possible that ***Phases 2*** and ***3*** represent dynamically derived combinations of Ti^{4+} rich and Ti metal phases.

Notably, the data treatment leading to the component spectra derived in this work does not yield unique solutions for these component spectra. Therefore, the conclusions drawn from applying these component spectra to data should be seen in this context, namely, other component spectra may offer different interpretations for these same sputter experiments. However, during the process of creating these component spectra, through observing how different photoemission peaks correlated with one another, it became apparent that shapes in photoemission spectra, even when shifted in binding energy, did not naturally suggest a change in stoichiometry. In this sense, investing time in and analysing these sputter experiments led to a hypothesis, that at the outset was not apparent.

CRediT authorship contribution statement

Pascal Bargiela: Writing – review & editing, Investigation. **Vincent Fernandez:** Writing – review & editing, Investigation. **David Morgan:** Writing – review & editing, Investigation. **Mireille Richard-Plouet:** Writing – review & editing. **Neal Fairley:** Writing – review & editing, Writing – original draft, Methodology, Conceptualization. **Jonas Baltrusaitis:** Writing – review & editing, Writing – original draft, Supervision, Methodology, Investigation, Conceptualization.

Declaration of competing interest

The authors declare that they have no known competing financial interests or personal relationships that could have appeared to influence the work reported in this paper.

Data availability

Data will be made available on request.

Acknowledgments

This work by JB was supported as part of Understanding & Controlling Accelerated and Gradual Evolution of Materials for Energy (UNCAGE-ME), an Energy Frontier Research Center funded by the U.S. Department of Energy, Office of Science, Basic Energy Sciences under Award # DE-SC0012577. The CNRS is acknowledged for financial support to the Thematic Workshop (N° 1317144) held at the Station Biologique, Roscoff, France. DJM acknowledges the EPSRC National Facility for XPS ("HarwellXPS", EP/Y023587/1, EP/Y023609/1, EP/Y023536/1, EP/Y023552/1 and EP/Y023544/1).

References

Atuchin, V.V., Isaenko, L.I., Khyzhun, O.Y., Pokrovsky, L.D., Sinelnichenko, A.K., Zhurkov, S.A., 2008. Structural and electronic properties of the $KTiOAsO_4$(001) surface. Opt. Mater. 30 (7), 1149–1152.

Baer, D.R., Shard, A.G., 2020. Role of consistent terminology in XPS reproducibility. J. Vac. Sci. Technol. A 38 (3), 031203.

Bala, J., Roy, S., John, A.T., Wadhwa, S., Mathur, A., Singh, D., Devi, D., Tripathi, A., 2020. Ion beam modified TiO_2 nanotubular bio-interface for electrochemical detection of L-tyrosine towards smart bandage application. Colloids Surf. B Biointerfaces 195, 111239.

Bargiela, P., Fernandez, V., Ravisy, W., Morgan, D., Richard-Plouet, M., Fairley, N., Baltrusaitis, J., 2024. Surface Analysis Insight Note: observations relating to photoemission peak shapes, oxidation state, and chemistry of titanium oxide films. Surf. Interface 56, 181–188.

Barlow, A.J., Portoles, J.F., Cumpson, P.J., 2014. Observed damage during Argon gas cluster depth profiles of compound semiconductors. J. Appl. Phys. 116 (5), 054908.

Biesinger, M.C., Lau, L.W.M., Gerson, A.R., Smart, R.S.C., 2010. Resolving surface chemical states in XPS analysis of first row transition metals, oxides and hydroxides: Sc, Ti, V, Cu and Zn. Appl. Surf. Sci. 257 (3), 887–898.

Byrne, C., Subramanian, G., Pillai, S.C., 2018. Recent advances in photocatalysis for environmental applications. J. Environ. Chem. Eng. 6 (3), 3531–3555.
Carley, A.F., Chalker, P.R., Riviere, J.C., Roberts, M.W., 1987. The identification and characterisation of mixed oxidation states at oxidised titanium surfaces by analysis of X-ray photoelectron spectra. J. Chem. Soc. Faraday Trans. 1 Phys. Chem. Condens. Phases 83 (2), 351.
Chambers, S.A., Engelhard, M.H., Wang, L., Droubay, T.C., Bowden, M.E., Wahila, M.J., Quackenbush, N.F., Piper, L.F.J., Lee, T.-L., Nelin, C.J., Bagus, P.S., 2017. X-ray photoelectron spectra for single-crystal Ti_2O_3 : experiment and theory. Phys. Rev. B 96 (20), 205143.
Chang, C.F., Koethe, T.C., Hu, Z., Weinen, J., Agrestini, S., Zhao, L., Gegner, J., Ott, H., Panaccione, G., Wu, H., Haverkort, M.W., Roth, H., Komarek, A.C., Offi, F., Monaco, G., Liao, Y.-F., Tsuei, K.-D., Lin, H.-J., Chen, C.T., Tanaka, A., Tjeng, L.H., 2018. c-Axis dimer and its electronic breakup: the insulator-to-metal transition in Ti_2O_3. Phys. Rev. X 8 (2), 021004.
Diebold, U., 2003. The surface science of titanium dioxide. Surf. Sci. Rep. 48 (5–8), 53–229.
Diebold, U., Madey, T.E., 1996. TiO_2 by XPS. Surf. Sci. Spectra 4 (3), 227–231.
Egelhoff, W.F., 1987. Core-level binding-energy shifts at surfaces and in solids. Surf. Sci. Rep. 6 (6–8), 253–415.
Fairley, N., Fernandez, V., Richard-Plouet, M., Guillot-Deudon, C., Walton, J., Smith, E., Flahaut, D., Greiner, M., Biesinger, M., Tougaard, S., Morgan, D., Baltrusaitis, J., 2021. Systematic and collaborative approach to problem solving using X-ray photoelectron spectroscopy. Appl. Surf. Sci. Adv. 5, 100112.
Fairley, N., Bargiela, P., Huang, W.-M., Baltrusaitis, J., 2023. Principal Component Analysis (PCA) unravels spectral components present in XPS spectra of complex oxide films on iron foil. Appl. Surf. Sci. Adv. 17, 100447.
Feng, H., Xu, Z., Ren, L., Liu, C., Zhuang, J., Hu, Z., Xu, X., Chen, J., Wang, J., Hao, W., Du, Y., Dou, S.X., 2018. Activating titania for efficient electrocatalysis by vacancy engineering. ACS Catal. 8 (5), 4288–4293.
Fernandes, R., Patel, N., Dholam, R., Adami, M., Miotello, A., 2009. Low energy ion-beam modification of TiO_2 photocatalyst thin film for visible light absorption. Surf. Coating. Technol. 203 (17–18), 2579–2583.
Fernandez, V., Morgan, D., Bargiela, P., Fairley, N., Baltrusaitis, J., 2023. Combining PCA and nonlinear fitting of peak models to re-evaluate C 1s XPS spectrum of cellulose. Appl. Surf. Sci. 614, 156182.
Fujishima, A., Zhang, X.T., Tryk, D.A., 2008. TiO_2 photocatalysis and related surface phenomena. Surf. Sci. Rep. 63 (12), 515–582.
Garland, B.M., Fairley, N., Strandwitz, N.C., Thorpe, R., Bargiela, P., Baltrusaitis, J., 2022. A study of in situ reduction of MoO_3 to MoO_2 by X-ray Photoelectron Spectroscopy. Appl. Surf. Sci. 598, 153827.
Gonbeau, D., Guimon, C., Pfister-Guillouzo, G., Levasseur, A., Meunier, G., Dormoy, R., 1991. XPS study of thin films of titanium oxysulfides. Surf. Sci. 254 (1–3), 81–89.
González-Elipe, A., Munuera, G., Espinos, J., Sanz, J., 1989. Compositional changes induced by 3.5 keV Ar+ ion bombardment in Ni-Ti oxide systems. Surf. Sci. 220 (2–3), 368–380.
Greczynski, G., Hultman, L., 2016. Self-consistent modelling of X-ray photoelectron spectra from air-exposed polycrystalline TiN thin films. Appl. Surf. Sci. 387, 294–300.
Haryński, Ł., Czylkowski, D., Hrycak, B., Karczewski, J., Gumieniak, J., Kramek, A., Ryl, J., Grochowska, K., Dors, M., Siuzdak, K., 2023. Nitrogen plasma-induced crystallization of anodic TiO_2 nanotubes for solar photoelectrochemistry. Appl. Surf. Sci. 615, 156472.
Jenko, M., Gorenšek, M., Godec, M., Hodnik, M., Batič, B.Š., Donik, Č., Grant, J.T., Dolinar, D., 2018. Surface chemistry and microstructure of metallic biomaterials for hip and knee endoprostheses. Appl. Surf. Sci. 427, 584–593.
Jiang, Z., Rhine, W.E., 1991. Preparation of titanium nitride (TiN) and titanium carbide (TiC) from a polymeric precursor. Chem. Mater. 3 (6), 1132–1137.
Kurtz, R.L., Henrich, V.E., 1998. Comparison of Ti 2p core-level peaks from TiO2, Ti2O3, and Ti metal, by XPS. Surf. Sci. Spectra 5 (3), 179–181.
Luthin, J., Linsmeier, C., 2001. Characterization of electron beam evaporated carbon films and compound formation on titanium and silicon. Phys. Scripta T91 (1), 134.
Majhi, R., Rajbhar, M.K., Das, P., Elliman, R.G., Chatterjee, S., 2022. Low energy ion beam-induced joining of TiO_2 nanoparticles. J. Alloys Compd. 924, 166440.
Mens, A.J.M., Gijzeman, O.L.J., 1996. AES study of electron beam induced damage on TiO_2 surfaces. Appl. Surf. Sci. 99 (2), 133–143.
Mohanta, R.R., Medicherla, V.R.R., Mohanta, K.L., Nayak, N.C., Majumder, S., Solanki, V., Varma, S., Bapna, K., Phase, D.M., Sathe, V., 2015. Ion beam induced chemical and morphological changes in TiO_2 films deposited on Si(111) surface by pulsed laser deposition. Appl. Surf. Sci. 325, 185–191.
Morgan, D.J., 2023. Core-level spectra of metallic lanthanides: dysprosium (Dy). Surf. Sci. Spectra 30 (2).
Oku, M., Wagatsuma, K., Kohiki, S., 1999. Ti 2p and Ti 3p X-ray photoelectron spectra for TiO_2, $SrTiO_3$ and $BaTiO_3$. Phys. Chem. Chem. Phys. 1 (23), 5327–5331.
Pabón, B.M., Beltrán, J.I., Sánchez-Santolino, G., Palacio, I., López-Sánchez, J., Rubio-Zuazo, J., Rojo, J.M., Ferrer, P., Mascaraque, A., Muñoz, M.C., Varela, M., Castro, G. R., de la Fuente, O.R., 2015. Formation of titanium monoxide (001) single-crystalline thin film induced by ion bombardment of titanium dioxide (110). Nat. Commun. 6 (1), 6147.
Pasquarello, A., Hybertsen, M.S., Car, R., 1996. Theory of Si 2 p core-level shifts at the Si (001)- SiO_2 interface. Phys. Rev. B 53 (16), 10942–10950.
Pelaez, M., Nolan, N.T., Pillai, S.C., Seery, M.K., Falaras, P., Kontos, A.G., Dunlop, P.S.M., Hamilton, J.W.J., Byrne, J.A., O'Shea, K., Entezari, M.H., Dionysiou, D.D., 2012. A review on the visible light active titanium dioxide photocatalysts for environmental applications. Appl. Catal. B Environ. 125, 331–349.
Ramana, C.V., Atuchin, V.V., Becker, U., Ewing, R.C., Isaenko, L.I., Khyzhun, O.Y., Merkulov, A.A., Pokrovsky, L.D., Sinelnichenko, A.K., Zhurkov, S.A., 2007. Low-energy Ar + ion-beam-induced amorphization and chemical modification of potassium titanyl arsenate (001) crystal surfaces. J. Phys. Chem. C 111 (6), 2702–2708.
Roberts, M.W., Tomellini, M., 1992. Mixed oxidation states of titanium at the metal-oxide interface. Catal. Today 12 (4), 443–452.
Sayers, C.N., Armstrong, N.R., 1978. X-ray photoelectron spectroscopy of TiO_2 and other titanate electrodes and various standard Titanium oxide materials: surface compositional changes of the TiO_2 electrode during photoelectrolysis. Surf. Sci. 77 (2), 301–320.
Scofield, J.H., 1976. Hartree-Slater subshell photoionization cross-sections at 1254 and 1487 eV. J. Electron. Spectrosc. Relat. Phenom. 8 (2), 129–137.
Sumita, T., Otsuka, H., Kubota, H., Nagata, M., Honda, Y., Miyagawa, R., Tsurushima, T., Sadoh, T., 1999. Ion-beam modification of TiO_2 film to multilayered photocatalyst. Nucl. Instrum. Methods Phys. Res. Sect. B Beam Interact. Mater. Atoms 148 (1–4), 758–761.
Tuckute, S., Varnagiris, S., Urbonavicius, M., Lelis, M., Sakalauskaite, S., 2019. Tailoring of TiO_2 film crystal texture for higher photocatalysis efficiency. Appl. Surf. Sci. 489, 576–583.
Zhan, X., Peng, Z., Huang, H., Zhang, H., Liu, Z., Ou, X., Yang, F., Liu, Z., 2021. Photoelectrochemical performance enhancement of low-energy Ar+ irradiation modified TiO_2. Appl. Surf. Sci. 541, 148527.